Assembly of Nanomaterials Through Highly Ordered Self-Assembled Monolayers and Peptide-Organic Hybrid Conjugat....

Article *in* Journal of Nanoscience and Nanotechnology · September 2007

DOI: 10.1166/jnn.2007.615 · Source: PubMed

CITATIONS
16

READS
159

10 authors, including:

Melvin T Zin
University of Washington Seattle
16 PUBLICATIONS **421** CITATIONS
SEE PROFILE

Hadi M Zareie
University of Technology Sydney
69 PUBLICATIONS **1,490** CITATIONS
SEE PROFILE

Seokho Kang
Dow Chemical Company
26 PUBLICATIONS **670** CITATIONS
SEE PROFILE

Journal of
Nanoscience and Nanotechnology
Vol. 7, 2549–2566, 2007

REVIEW

Assembly of Nanomaterials Through Highly Ordered Self-Assembled Monolayers and Peptide-Organic Hybrid Conjugates as Templates

Hong Ma, Melvin T. Zin, M. Hadi Zareie, Mun-Sik Kang, Seok-Ho Kang, Kyoung-Soo Kim, Bryan W. Reed, Candan Tamerler Behar, Mehmet Sarikaya*, and Alex K.-Y. Jen*

Department of Materials Science and Engineering, University of Washington, Box 352120, Seattle, Washington 98195, USA

Synthesis and processing techniques have now been established for obtaining high quality monodisperse nanocrystals of various metallic and semiconducting materials, fullerenes of distinct properties, single- and multi-wall carbon nanotubes, polymeric dendrimers with tailored functionalities, as well as other nanophase constructs. The next key step towards novel applications of nanostructured materials concerns their positioning, arrangement, and connection into functional networks without mutual aggregation. In this review, we highlight the recent progress of using anthracene- and pyrene-based self-assembling molecules with tunable energetic ($\pi-\pi$ interactions, hydrogen bonding, dipole–dipole interactions) and variable geometries to create stable, highly ordered, and rigid self-assembled monolayer (SAM) templates with adjustable superlattices on crystalline substrates. Based on aromatic SAM templates, stable and highly ordered self-assembled structures of optoelectronically active C_{60} have been obtained and shown to exhibit desirable electrical and optoelectronic properties, such as nonlinear transporting effect for molecular electronics and efficient photocurrent generation for mimicking photosynthesis in nature. By using genetically engineered polypeptides with surface recognition for specific inorganics, selective integration of nanoparticles onto aromatic SAM templates have also been realized. Through a combination of spatially confined surface chemical reaction and microcontact printing, sub-micron arrays of peptide-organic hybrid conjugates were successfully generated to serve as templates to achieve the patterned assembly of nanoparticles.

Keywords: Self-Assembled Monolayer, Genetically Engineered Protein, Nanomaterial, Molecular Electronics, Photocurrent Generation.

CONTENTS

1. INTRODUCTION

Nanostructured materials represent a fascinating class of materials whose structural elements such as atomic clusters, crystallites, or molecules have dimensions in the range of 1 to 100 nm, the length scale that defines physical properties of materials and at which intriguing phenomena are observed due to quantum phenomena. They exhibit unique electrical, optical, and magnetic properties that are readily tunable through controlling their size, and enable novel applications that are impossible to realize with their bulk counterparts. Synthesis and processing of nanostructured materials have come a long way. Methods have now been established to obtain monodisperse nanocrystals of various metallic and semiconducting materials,[1] fullerenes of distinct properties,[2] single- and multi-wall carbon nanotubes,[3] polymeric dendrimers with tailored functionalities,[4] as well as other nanophase constructs. The next key step towards novel applications

*Authors to whom correspondence should be addressed.

of nanostructured materials concerns their positioning, arrangement, and connection into functional networks without mutual aggregation. Among the bottom-up strategies, self-assembly provides a promising route to build up complex systems with immense flexibility in terms of nanoscale building blocks and resulting functionalities and properties.[5] As the name suggests, self-assembly is a process in which organization of colloidal, macromolecular, or supramolecule units into the desired system occurs through nature-intended phenomena, either mediated by physicochemical pathways or assisted by biomolecules to promote molecular selectivity and specificity.

In the beginning section of this paper, we highlight the design and synthesis of anthracene- and pyrene-based self-assembling molecules with tunable energetic (π–π interactions, hydrogen bonding, dipole–dipole interactions) and variable geometries to achieve stable, highly ordered, and rigid self-assembled monolayer (SAM) templates with adjustable superlattices on crystalline substrates. The following section focuses on the integration of nanostructured

Hong Ma received his Ph.D. degree in Organic Chemistry in 1997 from Nankai University, P. R. China. He worked as a postdoctoral researcher from 1997 to 2001 and a research scientist from 2001 to 2006 in Prof. Alex K.-Y. Jen's group at Northeastern University and the University of Washington, Seattle. He is currently a Research Assistant Professor in the Department of Materials Science and Engineering, University of Washington, where his research is focused mainly on the combination of molecular/biomacmolecular self-assembly and nanostructured materials for electronic, photonic, and biological applications.

Melvin T. Zin received his Bachelor of Science degree in Chemical Engineering from the University of Washington (Seattle, WA) in June 2002. He entered the doctoral program in the Department of Materials Science and Engineering at the University of Washington in September 2002 and is presently pursuing his Ph.D. studies under the direction of Professor Alex K.-Y. Jen. His research focuses on the directed self-assembly of nanomaterials via chemical and biomimetic templating and nanofabrication of plasmon resonant structures for surface-enhanced sensing and fluorescence.

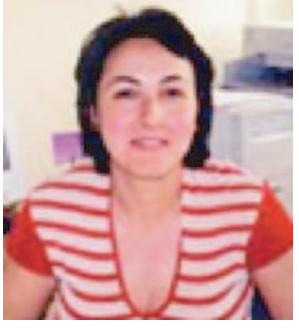

Candan Tamerler Behar received her Ph.D. in Chemical Engineering from Bogazici University, Istanbul, Turkey in 1997. She is currently Chair and Associate Professor in the Department of Molecular Biology and Genetics of Istanbul Technical University, Turkey. She is also Visiting Professor in the Department of Materials Science and Engineering, University of Washington. Her research focuses on molecular biomimetics, fungal enzymes, immobilized cell and enzyme systems, and production and purification of restriction enzymes.

Mehmet Sarikaya received his Ph.D. in Materials Science and Engineering from the University of California, Berkeley in 1982. He is currently Professor of Materials Science and Engineering, and affiliate Professor of Chemical Engineering at the University of Washington, Seattle. He is also the Director of the Genetically Engineered Materials Science and Engineering Center, a MRSEC sponsored by the National Science Foundation. Professor Sarikaya is a pioneer in molecular biomimetics. His research focuses on molecular biomimetics and genome-based molecular materials science and engineering; genetic engineering of inorganic-binding polypeptides (GEPI); fundamental phenomena at nano/bio interface; binding, specificity and assembly of engineered peptides; practical utilizations of GEPI as molecular erectors, assemblers and scaffolds in nanotechnology, medicine and energy.

Alex K.-Y. Jen received his Ph.D. in Chemistry from the University of Pennsylvania in 1984 under the tutelage of Professor Michael Cava. He started his career as a Research Chemist (1984–88) at Allied-Signal Inc., and joined Enichem America Inc. as a Principle Scientist in 1988. He moved to ROI Technology in 1995, where he served as the Vice President of the Materials Division. In 1997, he joined Northeastern University as an Associate Professor at the Department of Chemistry, moving to the University of Washington (UW) at Seattle in 1999 and was appointed as the Boeing-Johnson Chair Professor in the Department of Materials Science and Engineering. He is currently the Acting Chair of the department and has the joint appointment as a Professor in the Department of Chemistry. He was also appointed recently as the Founding Director of the Washington Institute on Advanced Materials Science and Technology. He was awarded as the AAAS Fellow and SPIE Fellow in 2005 for his pioneering contributions in the fields of molecular electro-optics and photonics. He has co-authored more than 370 papers and 40 patents and inventions in the interdisciplinary areas of organic functional materials and devices for opto-electronics, photonics, and molecularly- or biologically-inspired self-assemblies for sensing and electronics.

materials such as C_{60} onto the SAM templates to produce self-assembled structures with interesting properties such as potential negative differential resistance (NDR) effect for molecular electronics and efficient photocurrent generation for mimicking photosynthesis in nature. In the last section of this paper, we demonstrate the covalent immobilization of genetically engineered polypeptides onto the SAM templates for possible biotechnological applications, and the patterned assembly of nanoparticles using peptide-organic hybrid conjugates as templates for various bionanotechnological applications targeting bio/nano or bio/synthetic interphase.

2. EFFECTS OF MOLECULAR ARCHITECTURE, ω-FUNCTIONAL GROUPS, AND HYDROGEN-BONDING ON THE NANOSCALE FEATURES OF HIGHLY-ORDERED SAMs

In contrast to ultra-thin films made by molecular beam epitaxy or chemical vapor deposition, SAMs are ordered and oriented in a comparatively pre-determined way.[6] SAMs derived from organic molecules containing a thiol moiety on metal surfaces have attracted much attention because they are fundamentally interesting to surface science and their use in many practical applications. During the past two decades, SAMs based on aliphatic thiols have been extensively studied due to their potential to tailor surface properties[7] (wetting, adhesion, lubrication, etc.) and their importance in studying biomaterial interfaces,[8] biosensing,[9] cell growth,[10] crystallization,[11] and many other systems.[12] Therefore, SAMs prepared from *n*-alkanethiols and ω-functionalized alkanethiols are relatively well-characterized and well-understood. On the other hand, SAMs of aromatic thiols have been studied only in recent years for potential applications in electronics[13–18] and photonics[19] due to their π-conjugated character. The development of stable and highly ordered SAMs with controllable nanoscale features is crucial for exploring the charge injection/transport mechanisms in molecular electronics, organic/polymer electronics/optoelectronics, and molecular recognition.

In order to govern the formation of self-assembled structures, one has to understand the driving force (molecule–molecule interactions, adsorbate–substrate interactions) for two-dimensional (2D) self-assembly is required. However, such driving force for self-assembly has been studied using limited kinds of adsorbates. There have been few general arguments about the geometry and energetics on the formation of stable and highly ordered SAMs using other kinds of adsorbates. We have designed and synthesized several series of fused-ring aromatic self-assembling molecules to have variable geometries through different molecular architectures, ω-functional groups, and hydrogen bonding moieties, and thus to possess tunable energetics from molecule–molecule interaction such as van der Waals attractions, $\pi-\pi$ interactions, hydrogen bonding, and dipole–dipole interactions. By balancing the energetics of molecule–molecule interaction and adsorbate–substrate interaction, stable and highly ordered SAMs with adjustable nanoscale features have been realized.

2.1. Effect of Molecular Architecture

To systematically investigate the nanoscale features of SAMs from aryl derivatives, we have designed and synthesized three molecules with significantly different molecular architectures as shown in Figure 1. They are: (4-mercaptophenyl)phenylacetylene (MPPA), (4-mercaptophenyl)(9-anthryl)acetylene (MPAA), and (4-mercaptophenyl)(1-pyryl)acetylene (MPPYA). The first molecule, MPPA, has been previously studied, whereas the other two molecules, MPAA and MPPYA, are newly designed. All three molecules possess phenylacetylene moiety, but the incorporation of fused aromatic rings leads to systematically varied molecular dimensions—1.26×0.43 nm for MPPA, 1.26×0.92 nm for MPAA, and 1.47×0.80 nm for MPPYA based on MM2 calculation and numbers of π-electrons (6, 14, and 16 for phenyl, anthryl, and pyryl, respectively). STM characterizations revealed that

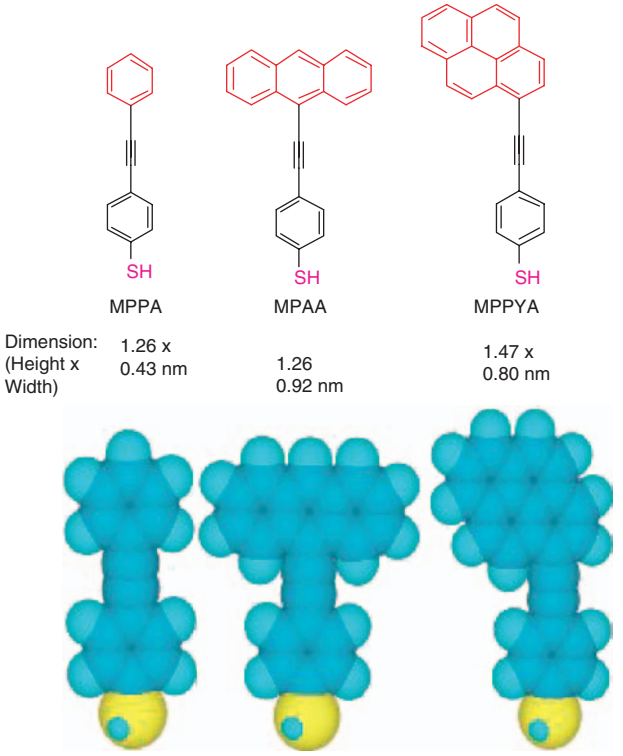

Fig. 1. Structures and dimensions of the three molecules based on MM2 calculations.

the molecular architecture of MPPA, MPAA, and MPPYA drastically affects the nanoscale features of their SAMs on Au(111) substrate. SAMs from fused-ring aromatics such as anthryl- or pyryl-based molecules become both densely packed and highly ordered compared to phenyl-based molecules due to increased intermolecular π–π interactions generated by fused aromatic rings. Furthermore, we observed that the unit cell parameters of SAMs on Au(111) substrate depend on molecular architecture and time-related organization instead of $\sqrt{3}a \times \sqrt{3}a$ commonly observed for alkanethiols. With extended self-assembly time, the anthryl-based molecules form 2D arrays or stacked pseudo-1D wires while the pyryl-based molecules stabilize into a periodic pattern with a dimerized structural unit. This provides an effective way to control the nanoscale features of SAMs from aryl derivative by manipulating their molecular architecture and thus their intermolecular π–π interactions.

Self-assembling characteristics of MPPA, MPAA, and MPPYA were dynamically studied using surface plasmon resonance (SPR) spectroscopy as presented in Figures 2(A–C). The SPR spectrum corresponds to time-dependent wavelength shift as a result of the increase in surface coverage of adsorbing molecules onto the gold substrate in ethanolic solution at room temperature. At time zero, ethanol was injected to establish a baseline, after which the solution of molecules was introduced to initiate chemisorption onto the gold substrate, followed

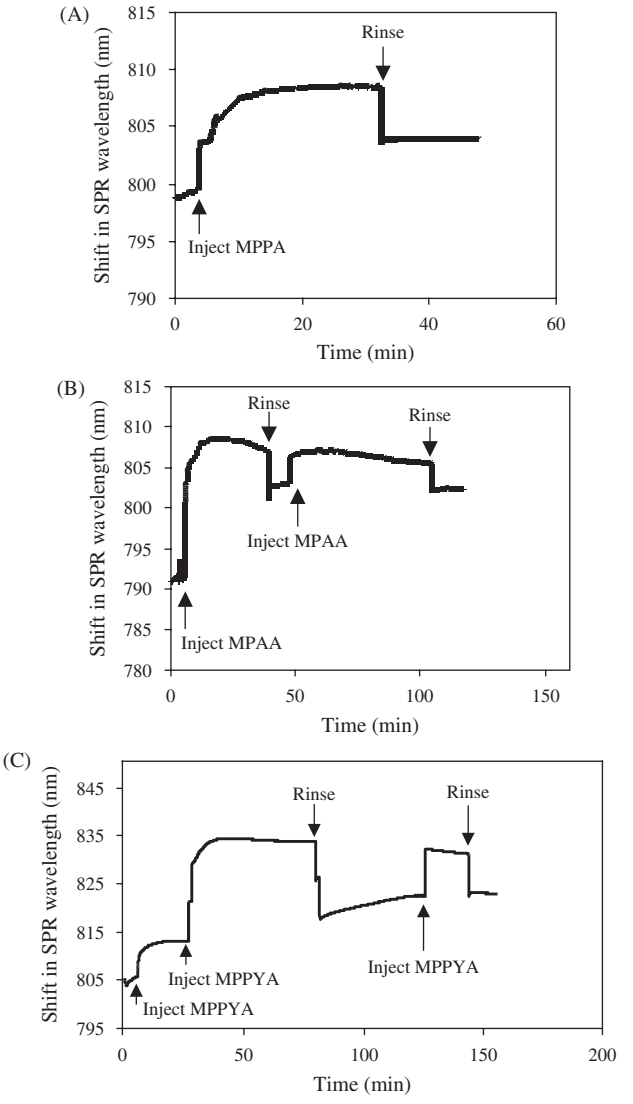

Fig. 2. SPR profiles of the molecules adsorbed on polycrystalline gold substrates: SPR wavelength shift versus assembly time; (A) MPPA; (B) MPAA; and (C) MPPYA.

by their reorganization to achieve a SAM in the thermodynamically stable configuration. Since total wavelength shift (with respect to the baseline) is correlated to surface coverage of molecules, relative surface coverage of MPPA, MPAA, and MPPYA can be determined from relative wavelength shifts in their SPR profiles. In Figure 2(A), after establishing the baseline, the solution of MPPA was injected (left arrow indicates the time of injection). Consequently, the formation of SAM on the gold substrate results in a rapid wavelength shift in the SPR spectrum. After 35 min, ethanol is injected (right arrow) to rise off the physisorbed molecules from the gold substrate. Removal of excess molecules is reflected by a sharp drop in the wavelength shift. The absolute wavelength shift can be computed to obtain the amount of chemisorbed molecules. For example, wavelength shift of 4.97 nm

corresponds to $3.25 \pm 0.21 \times 10^{14}$ MPAA molecules per cm^2 on the gold substrate (calculated according to the well-known protocol in Ref. [20]). SPR analysis of the self-assembly of MPAA is given in Figure 2(B). In this case, injection/rinsing cycle was repeated twice—first rinsing after 10 minutes and last rinsing after 110 minutes. In this case, because of the increased intermolecular π–π interactions among MPAA molecules, multiple injection/rinsing procedure was necessary to ensure the removal of excess molecules from the gold substrate. The final saturation level gives a wavelength shift of 10.90 nm, corresponding to a surface coverage of $4.68 \pm 0.36 \times 10^{14}$ MPAA molecules per cm^2. Multiple injection/rinsing procedure was also applied to the self-assembly of MPPYA (Fig. 2(C)). Solution of molecules was injected three times and ethanol was injected twice to rinse off physisorbed molecules. In this case, the saturation level is reached at a wavelength shift of 16.94 nm, corresponding to $7.35 \pm 0.12 \times 10^{14}$ MPPYA molecules per cm^2. SPR characterizations of the self-assembly of MPAA and MPPYA imply that the anthryl- or pyryl-based molecules attained higher surface coverage (i.e., number of molecules per area) at their saturation level in comparison to the phenyl-based molecules reported to date. Denser packing of molecules within the SAM may be attributed to the increased intermolecular π–π interactions mediated by the fused-ring aromatics in their molecular architecture.

Common characteristic of SAMs from MPPA, MPAA, and MPPYA after 24-h immersion is the formation of their oblique lattice on Au(111) substrate (Figs. 3-(1)-A, B and 3-(3)-A, B). However, unit cell parameters of these SAMs are noticeably different. Non-hexagonal packing of these molecules is probably due to their molecular architectures which results in molecular footprints with large aspect ratios. Due to STM-tip convolution, the shapes of individual molecules with the SAMs are not fully discernable. Nevertheless, based on STM characterization, the unit cell parameters—$a \times b$ and θ—of the SAMs (modeled in Figs. 4A, B, and D) are determined to be: $0.97 \times 1.05 \pm 0.1$ nm, $46 \pm 2°$; $0.90 \times 1.00 \pm 0.1$ nm, $74 \pm 2°$; and $1.13 \times 0.80 \pm 0.2$ nm, $71 \pm 2°$ for MPPA, MPAA, and MPPYA, respectively. Variations between STM scans of the same

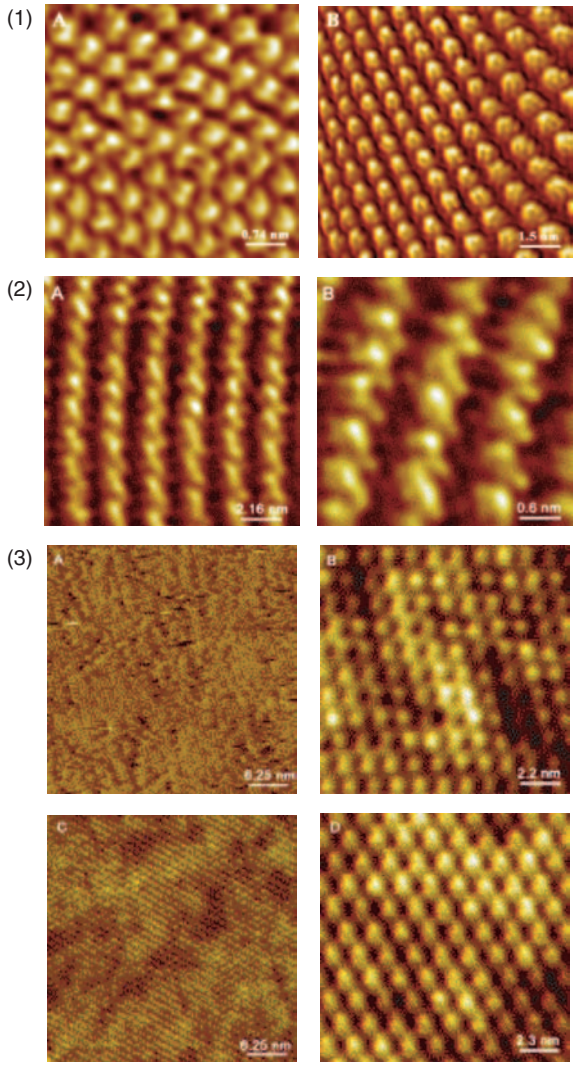

Fig. 3. (1) STM images of ordered assemblies of MPPA (A) and MPAA (B) after 24-h of assembling. (2) STM images (A and B) are from the new crystalline assembly of the MPAA molecules after soaking gold substrate in solution beyond 48 h. (3) STM images of ordered self-assemblies of MPPYA (A) after 24-h of assembling, (C) after 48-h of assembling, and (B), (D) magnified images of (A), (C), respectively. Reprinted with permission from [23], M. H. Zareie et al., *Nano Lett.* 3, 139 **(2003)**. © 2003, ACS, Washington, D.C.

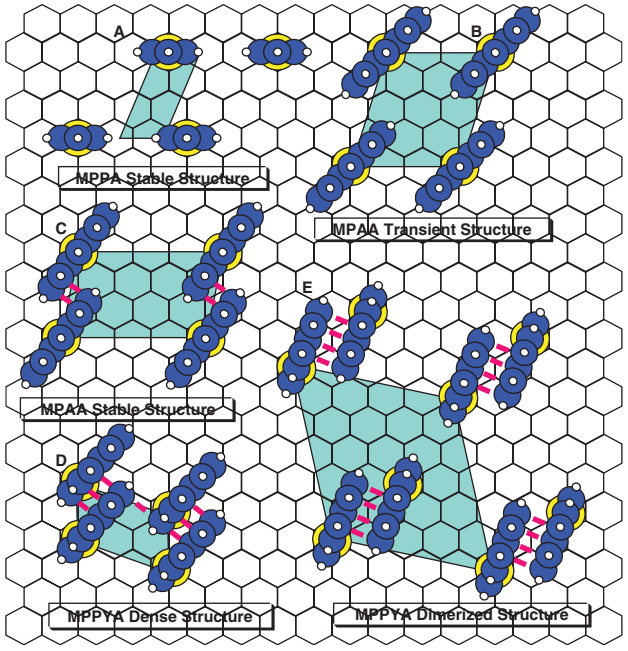

Fig. 4. Schematic real-space adsorbate unit cells of MPPA, MPAA, and MPPYA. (A) MPPA stable structure after 24- or 48-h self-assembling, (B) MPAA transient structure after 24-h self-assembling, (C) MPAA stable structure after 48-h self-assembling, (D) MPPYA dense structure after 24-h self-assembling, and (E) MPPYA dimerized structure after 48-h self-assembling.

sample gave rise to the uncertainty in the values of the unit cell parameters. Because of strong intermolecular π–π interactions and significantly different molecular architecture (in terms of shape and symmetry) of aromatic thiols in comparison to aliphatic thiols, different unit cell parameters of the SAMs are expected. However, differences in unit cell parameters could not be predicted. Assuming an atomically flat Au(111) substrate without surface reconstructions, unit cell parameters of SAMs correspond to $\sqrt{13}a \times 3a$, 46; $\sqrt{13}a \times 3a$, 74; and $\sqrt{3}a \times \sqrt{7}a$, 71 ($a = a\ (111) = 0.288$ nm) for MPPA, MPAA, and MPPYA, respectively, with an area ratio of 9:12:4 (with 9, 12, and 4 Au surface atoms per unit cell).

Finally, we studied the self-assembly dynamics and time-dependent organization of the molecules. While the SAM of MPPA was stable beyond 24 h, both MPAA and MPPYA slowly reorganize into more stable SAMs after 48 h (Figs. 3-(2)-A, B and 3-(3)-C, D), after which their SAMs remain unchanged (i.e., in the lowest thermodynamic configuration). Based on STM analysis,

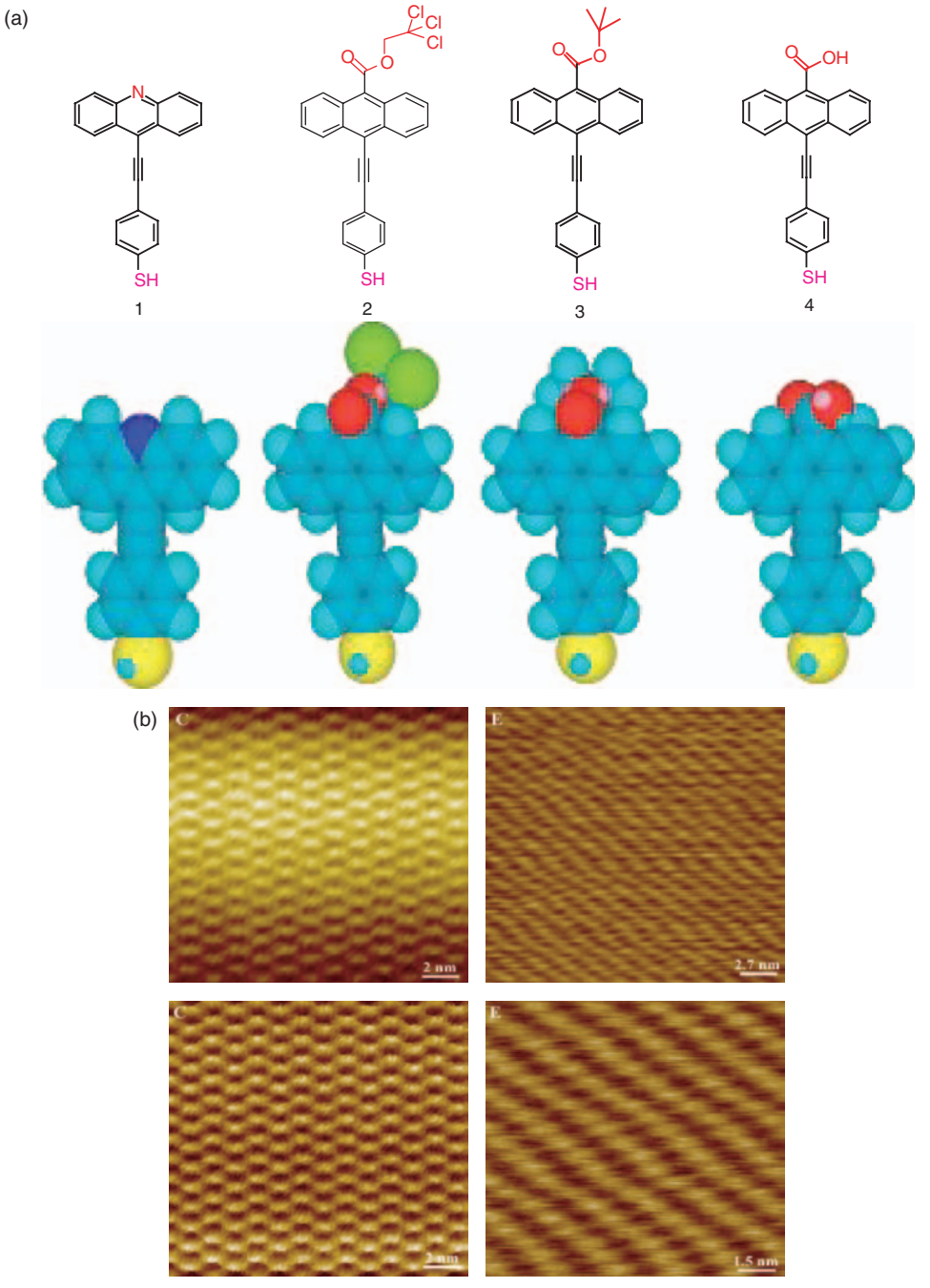

Fig. 5. (a) Molecular structures of 1–4. (b) STM images of ordered self-assemblies of molecule 1, left top: after 24-h of assembling, right top: after 48-h of assembling; molecule 2, left bottom: after 24-h of assembling, right bottom: after 48-h of assembling.

transformation within the SAM of MPAA results in a new set of unit cell parameters: $0.85 \times 1.25 \pm 0.05$ nm and $78 \pm 2°$. This is compatible with a $\sqrt{7}a \times 4a$ superlattice for MPAA on the Au(111) substrate (Fig. 4(C)). Similarly, the SAM of MPPYA has a new set of unit cell parameters, $1.50 \times 1.40 \pm 0.1$ nm and $68 \pm 2°$, corresponding to a $2\sqrt{7}a \times \sqrt{21}a$ superlattice on the Au(111) substrate (Fig. 4(E)).

2.2. Effect of ω-Functional Groups

A SAM presenting ω-functional end-groups in a predetermined fashion at the surface constitutes chemically well-defined interface for fundamental studies (for example, friction) and technological applications (for example, assembly of nanomaterials, platform for sensors). However, SAMs from alkanethiols results in surface reconstructions due to trans-gauche conformational changes in chain termina. This is especially noticeable in alkanethiols with ω-functional end-groups. Recently, we have designed and synthesized a series of fused-ring aromatic thiols (1, 2, 3, and 4) with ω-functional end-groups to systematically investigate their effects on the nanoscale features of SAMs. The introduction of acridine, ester, and carboxylic moieties leads to an increase in the molecular dipole moment in all four molecules. The bulky ester end-groups in 2 and 3 result in steric hindrance while the carboxylic end-group in 4 causes the tendency to form a dimer. Hence, from energetic and geometric perspectives, the introduction of both ester and carboxylic end-groups should lead to a disorder within the SAM. However, the SAMs from anthryl-based molecules are negligibly affected by their ω-functional end-groups due to the dominant intermolecular π–π interactions.

2.3. Effect of Hydrogen-Bonding

In order to study the effect of hydrogen-bonding on the nanoscale features of SAMs from aryl derivatives, a series of fused heterocyclic aromatic thiols (5, 6, 7, and 8) are self-assembled on the Au(111) substrate. The molecular frames are kept similar while the hydrogen-bonding moieties are increased. As shown in Figure 6, the best ordering within the SAM is achieved with 8, which has the most hydrogen-bonding moieties. The amino end-groups on the highly-ordered SAMs can be used to immobilize peptides or to assemble nanomaterials and functional nanostructures.

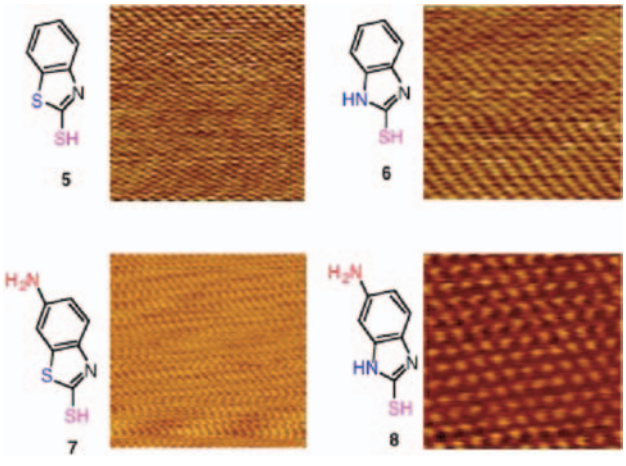

Fig. 6. STM images of ordered self-assemblies of 5 (7×7 nm), 6 (7×7 nm), 7 (6.5×6.5 nm), and 8 (4×4 nm) after 48-h of assembling.

3. HIGHLY-ORDERED SAMS WITH C_{60} FOR MOLECULAR ELECTRONICS AND OPTOELECTRONICS

Recently, multi-component SAMs and laterally structured SAMs have attracted a lot of attention due to their functional properties and pattern formation.[5b] In particular, heterostructures combining SAMs as templates with polymers, biomolecules, inorganic nanomaterials, and π-conjugated molecules have potential applications in "brush-like" coatings, biosensing, electronics, and photonics. Therefore, it is essential to form stable and highly ordered heterostructured SAMs to study the mechanisms for molecular electronics, organic/polymer electronics and optoelectronics, and molecular recognition. In this section, we highlight the development of highly ordered heterostructured SAMs with remarkable stability for potential applications in molecular electronics and photocurrent generation.

C_{60} molecule possesses unique electrical and optical properties due to its nanoscale structure, spherical shape, and uniformity.[21] The development of C_{60}-based materials relies on the novel methodologies for chemically modifying C_{60} molecule. Such methodologies include not only tailoring C_{60} to exhibit desirable electrical or optical response but also covalent attachment of C_{60} to substrates. Self-assembly of C_{60}-based molecules is a promising route to achieve ultra-thin films and to investigate their electrical and optical properties on substrates. During the last decade, several approaches such as alkanethiol chemistry, bipyridine binding, and low-temperature adsorption have been used to construct SAMs of C_{60}-based molecules on the gold substrate. However, it is difficult to simultaneously achieve nanoscale ordering and exceptional stability.[22] We have found that the anthryl-based self-assembling molecule, MPAA, can form stable and highly ordered SAMs due to strong π–π interactions generated by the fused aromatic rings.[23] Depending on the time of self-assembly, SAM of MPAA molecules transforms from ordered two-dimensionally stacked arrays to pseudo-one-dimensional wires (Figs. 7(A, B)). Consequently, we have verified that the conducting behavior of the SAMs of MPAA molecules depends on their local ordering. As shown in Figure 7(C), long-term configuration of MPAA SAM forms linear (wire-like) chained structures with

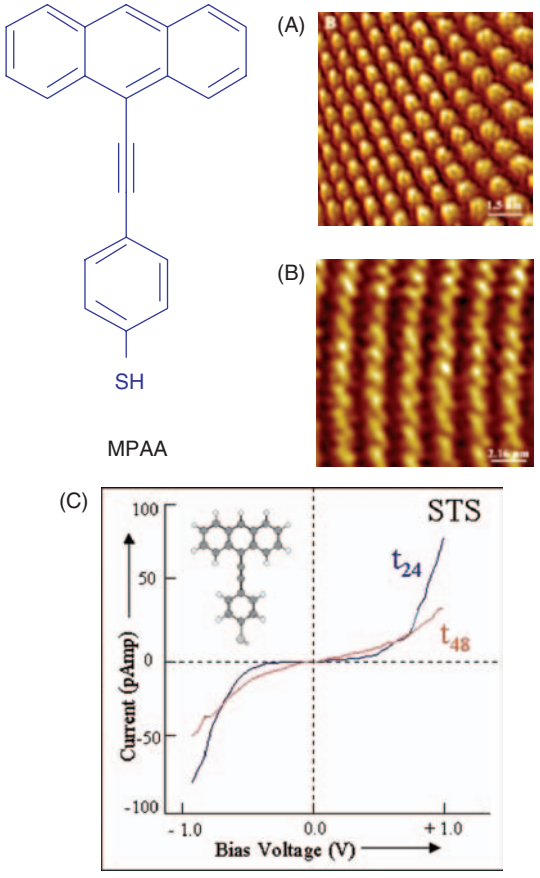

Fig. 7. STM images of the ordered self-assemblies of MPAA (A) after 24-h self-assembling, (B) after 48-h self-assembling, (C) I/V characteristics of MPAA in the SAMs after 48-h ordering compared to that after 24-h assembly. Reprinted with permission from [23], M. H. Zareie et al., *Nano Lett.* 3, 139 **(2003)**. © 2003, ACS, Washington, D.C.

improved conductivity and smaller energy gap compared to its transient (short-term) configuration. These intriguing phenomena are consistent with the results of quantum-chemical calculations.[24] The electronic properties change with respect to the energy levels of HOMO and LUMO states of the molecules in the ensemble; and energy differences between HOMO and LUMO states are consistent with the arrangement and packing of the molecules. These differences lead to different electron injection/transport mechanisms within these SAMs and are manifested in different conduction behaviors of these molecular wires. To account for some of the variations in the STS curves, molecule–substrate interactions may be taken into consideration. One could expect superlattices of the conducting molecules with different lattice vectors to modify the gold surface electronic states in different ways.[25] These interesting observations would warrant a new line of future research, both experimental and theoretical, to more quantitatively assess structure-property correlations to provide design guidelines for molecular design for electronics and photonics.

In order to combine the physical and chemical properties of C_{60} with the nanoscale ordering of anthryl-based

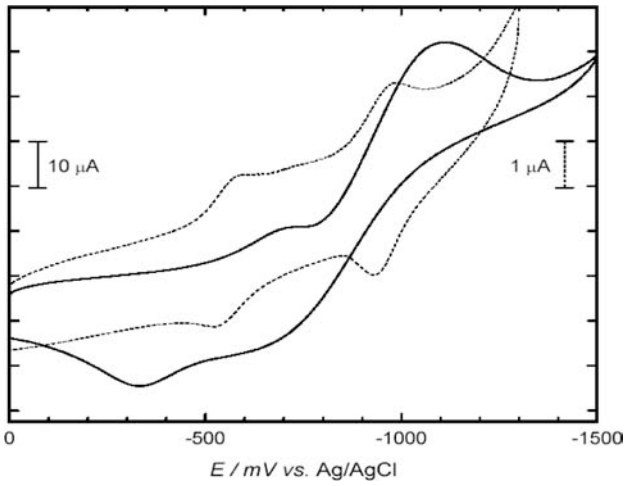

Fig. 8. Cyclic voltammetry curves of C_{60}-MPAA (dot line) and a SAM of C_{60}-MPAA (solid line) on gold substrate (toluene/acetonitrile (4:1) as the solvent, 0.1 M Bu_4NPF_6 as the electrolyte). Reprinted with permission from [26], S. H. Kang et al., *Angew. Chem. Int. Ed.* 43, 1512 **(2004)**. © 2004, WILEY-VCH Verlag GmbH & Co., KGaA, Weinheim.

SAMs, we have designed and synthesized C_{60}-MPAA hybrid molecule.[26] From cyclic voltammetry curves at room temperature (Fig. 8), C_{60}-MPAA hybrid molecule and SAM of C_{60}-MPAA on gold show two typical electrochemically accessible and stable oxidation states of C_{60}, respectively.[27]

Figure 9(A) shows a high-resolution STM image of the C_{60}-MPAA SAM on the Au(111) substrate at room temperature. Each bright spot indicates where a C_{60} molecule locates directly on top of an MPAA molecule. The image reveals a well-ordered 2D nanostructure that extends throughout a given textured Au(111) terrace. As shown in the reconstructed image using the Fourier transform of the periodic pattern shown in Figure 9(A), the organization of the hybrid molecules in the self-assembled structure exhibits a pseudo-hexagonal arrangement. The oblique lattice of the self-assembled structure from the hybrid molecules is characterized by a unit cell with $a = 1.00 \pm 0.25$ nm, $b = 0.90 \pm 0.25$ nm, and $\theta = 62 \pm 0.5°$. It is well-known that the self-assembly of C_{60} molecules on Au(111) substrate results in the formation of perfectly hexagonal lattice with a lattice parameter of about 0.9 nm.[28–31] The observation that the C_{60}-MPAA hybrid molecules does not form perfectly hexagonal lattice requires further consideration.

C_{60} molecule has a spherical shape. On a flat surface, spheres self-assemble into a hexagonal lattice, the lowest thermodynamic configuration, with a six-fold symmetry. However, as shown in Figure 9(A), the C_{60}-MPAA hybrid molecule self-assembles into an oblique lattice with a two-fold symmetry. This may be attributed to the asymmetric molecular architecture of the hybrid molecule—the planar MPAA part is slightly larger than the C_{60} part. While C_{60} alone has a full 360° rotational freedom, it is

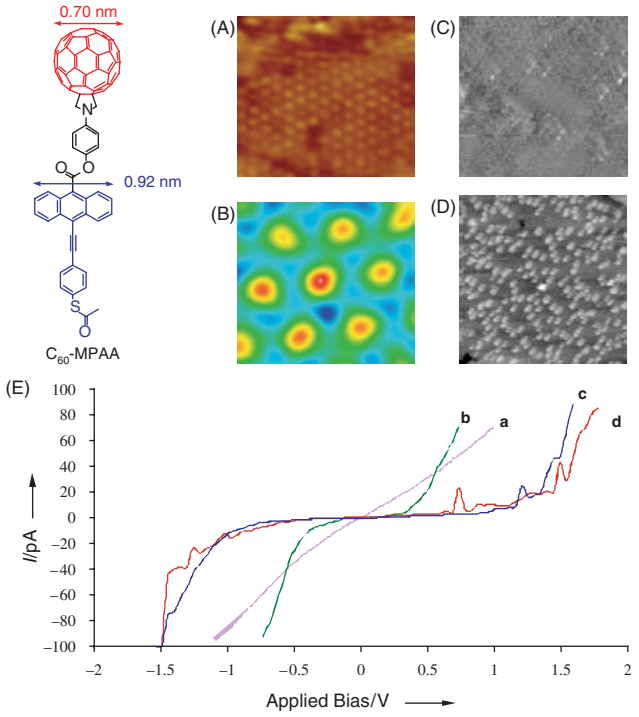

Fig. 9. STM images of the ordered self-assemblies. (A) After 24-h self-assembling of C_{60}-MPAA (15 × 15 nm); (B) reconstructed image using the Fourier transform of the periodic pattern shown in (A) reveals an oblique lattice (2.3 × 2.3 nm); (C) Assembly of C_{60}-MPAA observed after 24-h (40 × 40 nm); (D) Co-assembly of C_{60}-MPAA and MPAA (ratio of compositions: 1:9) after 24-h (15 × 15 nm). The bright spots in (D) corresponds to the aggregates of C_{60}-MPAA. (E) I/V characteristics of SAMs; a: Au(111); b: C_{60} only; c: homo-assembly for 24 h; d: co-assembly for 24 h. Reprinted with permission from [26], S. H. Kang et al., *Angew. Chem. Int. Ed.* 43, 1512 (**2004**). © 2004, WILEY-VCH Verlag GmbH & Co., KGaA, Weinheim.

restrained when it is tethered to the MPAA molecule and organized into a 2D self-assembled structure. Therefore, the two-fold symmetry imposes a restriction on the rotational freedom and forces the hybrid molecule into an oblique lattice which corresponds to the lowest thermodynamic configuration where centrally symmetric interactions among C_{60} molecules and planar interactions among MPAA molecules are compromised. From our earlier study,[23] it has been demonstrated that the SAM from MPAA molecules has an oblique lattice with unit cell parameters ($a = 0.76$ nm and $b = 1.15$ nm) which are significantly different from the lattice formed by the SAM from C_{60}-MPAA hybrid molecules.

Dimensions of the lattices formed by C_{60} alone and C_{60}-MPAA hybrid molecule are different, providing clues to their relative stabilities. For example, a C_{60} film deposited directly onto the Au(111) substrate shows a close-packed but unstable self-assembled structure composed of mobile hexagonal arrays with an intercluster spacing of 1.1 nm.[28–31] In addition, many other self-assembled structures based on alkanethiol-terminated fullerenes, fullerene-phenanthrolines, and disulfide-terminated fullerenes have been reported. However, their stability and ordering are not nearly comparable to the SAM of C_{60}-MPAA molecules. This is possibly due to the chain dynamic within the SAMs of alkanethiols, resulting in a loosely packed long-range organization.[32–36] Recently, it was reported that ordered C_{60} molecules can be formed on top of the SAM of alkyl thiols on the Au(111) substrate at 5 K.[37–38] In this case, the C_{60} molecules form close-packed hexagonal arrays with a nearest neighbor distance of 1.0 nm. However, the resulting self-assembled structures of C_{60} are not stable at room temperature. This instability is probably due to the detachment of C_{60} molecules from the alkyl thiols along with their free rotation above the SAM film. In our work, the SAMs of the hybrid molecules, which are made up of C_{60} covalently bonded to MPAA, exhibit a high degree of ordering and stability even at room temperature. The stable and robust nanoscale self-assembly and the resulting self-assembled structure is a result of the interplay of intermolecular interactions among π–π stacked MPAA molecules in addition to interactions among the C_{60} molecules and the thiol-Au bonding.

We have also prepared composite samples of C_{60}-MPAA hybrid molecules and MPAA molecules and observed their co-assembly to assess their structures and corresponding electrical properties. Figure 9(D) reveals co-assembled structures of C_{60}-MPAA hybrid molecules (10%) with MPAA molecules (90%). The C_{60}-MPAA molecules form stable island-like aggregates that are fairly homogeneously distributed within the matrix of highly ordered MPAA molecules. The bright spots in Figure 9(D) represents the constant current STM images of the hybrid molecules that are taller than the matrix molecules (2.98 nm versus 1.2 nm). The C_{60}-MPAA islands in Figure 9(D) contain smaller number of molecules (1 to 3) and appear to commensurate with the surrounding matrix of highly ordered MPAA molecules, possibly a result of the two-fold symmetry of the MPAA molecule in both regions.

We have investigated electronic behavior of the C_{60}-MPAA SAMs by establishing their current/voltage (I/V) characteristics by scanning tunneling spectroscopy (STS) (Fig. 9(E)). Curves a, b, and c in Figure 9(E) show the I/V characteristics of bare Au(111) substrate, physically adsorbed C_{60} monolayer, and homo-assembled monolayer of C_{60}-MPAA on Au(111) substrate, respectively. Curve d in Figure 9(E) exhibits the I/V characteristics of the SAM of C_{60}-MPAA co-assembled with MPAA. The I/V curves of C_{60}-MPAA in both homo-assembly and co-assembly show semiconducting behavior, evident when compared with the metallic characteristic of bare Au(111) substrate. The C_{60}-MPAA molecule, whether homo-assembled or co-assembled, has a much larger energy gap than the C_{60} alone when it is directly adsorbed on the Au(111) substrate through physisorption. This is probably due to the fact that the introduction of anthrylphenyl acetylene moiety changes the electronic characteristics of the C_{60} which

is verified by UV-vis absorption spectra. Moreover, the STS spectra of the C_{60}-MPAA show multiple peaks in I/V curves (Fig. 9(E), curves c and d). These peaks resemble NDR phenomenon reported by Reed et al.[39] The occurrence of potential NDR effect is possibly due to the weak charge transfer between the MPAA and the electron-affinitive C_{60} at the molecular junction of C_{60}-MPAA. It should be noted that the I/V curves of the SAMs of neither C_{60} nor MPAA[23] alone exhibit these peaks.

Another interesting point to note in the I/V curves corresponding to C_{60}-MPAA molecules in both homo and mixed states is that only weak (or no) apparent NDR-type peaks appear on the negative bias side. This finding may be an indication that charge transfer takes place more strongly in one direction, i.e., from the electron-rich MPAA to the electron-deficient C_{60}. Moreover, these peaks exhibit very different bias voltage positions in the homo- and co-assembled SAMs of C_{60}-MPAA (curves c and d in Fig. 9(E)). The multiple peaks in I/V curves are especially clear in the co-assembly state (Fig. 9(E), curve d) possibly because of the measurements from isolated islands of C_{60}-MPAA. The differences in the characteristic of the peaks (number of peaks and their positions) may be due to a collective phenomenon of different molecular surroundings of the C_{60}-MPAA molecules and their local ordering within the two SAMs, leading to different molecular orbitals of the two self-assembled structures. The more in-depth investigation of the electrical properties of these SAMs, especially the verification of the possible NDR effect, could be carried out through STS measurements of the I/V characteristics by carefully isolating the hybrid molecules within the MPAA matrix, as planned in the near future.

To further explore the C_{60}-MPAA hybrid molecule, we have investigated the efficiency of photocurrent generation from their self-assembled structures. The photoelectrochemical measurements were conducted in a Na_2SO_4 solution (0.1 M) containing 50 mM methyl viologen (MV^{2+}) as an electron carrier. Either bare Au substrate or modified Au substrate with C_{60}-MPAA was used as a working electrode, with platinum as a counter electrode and Ag/AgCl as a reference electrode in the test configuration of Au/C_{60}-MPAA/MV^{2+}/Pt. The photocurrent was immediately generated when a white light source was used to illuminate the SAM of C_{60}-MPAA in electrolyte solution and the initial value of photocurrent went down instantly when the illumination was terminated. As shown in Figure 10, photocurrent responses were recorded under the illumination of a white light source with 260 mW/cm^2 intensity. When Au/C_{60}-MPAA/MV^{2+}/Pt was irradiated under a bias voltage of −100 mV/s versus Ag/AgCl, a stable cathodic photocurrent (ca. 1600 nA/cm^2) was generated, whereas the photocurrent response from a bare gold electrode was negligible under the same illumination. Figure 11 shows the photocurrent generation upon

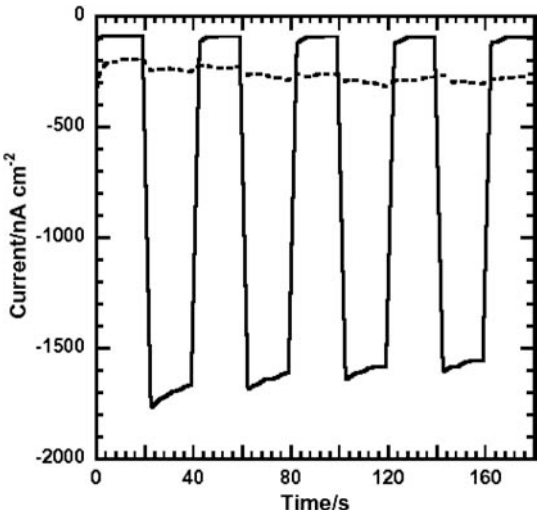

Fig. 10. Light-induced "ON"–"OFF" switchable photoelectrochemical response of bare Au/MV^{2+}/Pt (dotted line) and Au/C_{60}-MPAA/MV^{2+}/Pt (solid line), Ag/AgCl (saturated KCl) as reference electrode, Pt as counter electrode, electrolyte: 0.1 M Na_2SO_4 containing 50 mM methylviologen (MV^{2+}) with white light of 260 mW/cm^2 at −100 mV versus Ag/AgCl.

the application of different bias potentials on the electrode. The semi-linear increase of the cathodic photocurrent with the increase of negative bias (from +200 mV to −200 mV versus Ag/AgCl) to the gold electrode demonstrates that the photocurrent flows from the gold electrode to the counter electrode through the SAM and the electrolyte. The cathodic photocurrent dramatically increased as the potential bias is lowered below +100 mV. However, a further increase of negative bias beyond −300 mV to the gold electrode could not be realized due to a significant increase of the cathodic current as the dark current. The quantum yield of 14% was obtained for the

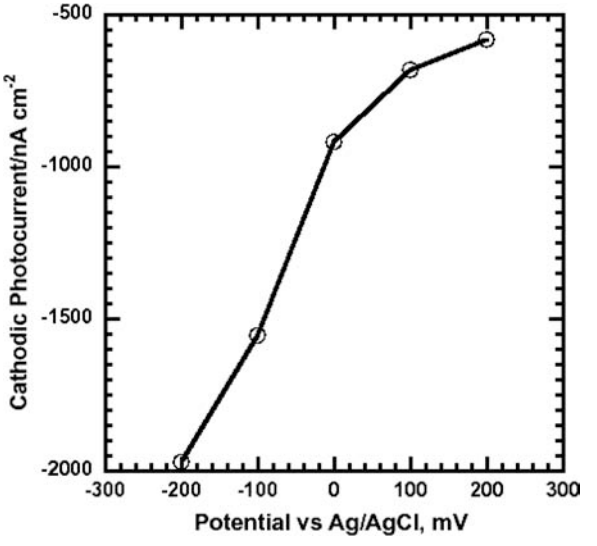

Fig. 11. Photocurrent versus applied potential curve for the Au/C_{60}-MPAA/MV^{2+}/Pt with white light of 260 mW/cm^2.

photocurrent generation from C_{60}-MPAA SAM on gold with a monochromatic wavelength of 400 nm,[40a] indicating their promise for mimicking photosynthesis in nature.

As an extension of the investigation on photocurrent generation, C_{60}-tethered 2,5-dithienylpyrrole triad was synthesized and assembled on gold.[40b] The three-electron reduced C_{60} radical anions of the triad both in solution and as SAM were detected at room temperature. The photocurrent generated in a (Au/C_{60}-triad/MV^{2+}/Pt) cell upon irradiation of light is exceptionally large (3200 nA/cm^2) with high quantum yield (51%). The electron-rich characteristics of the molecular architecture and the rigid conjugated molecular framework stabilize the C_{60} radical anions generated during electrochemical reduction and lead to a remarkable enhancement of photocurrent generation. A novel self-assembling molecule with coplanar anthraquinonyl and anthryl moieties linked by an acetylenic unit has also been designed and synthesized as an electron acceptor for efficient photocurrent generation.[41] STM characterization reveals that the SAM of this molecule forms highly ordered 2-D arrays on the Au(111) substrate with an oblique lattice with graphite-like stacking at room temperature. The electrochemical study of this molecule and its SAM showed reversible characteristics. The SAMs formed by co-assembling this acceptor with an oligo(pyrrolethiophene) donor show very promising photochemical properties. The amount of photocurrent generated (up to 1425 nA/cm^2 with quantum yield of 23.1%) under the illumination of 360 nm light is comparable to that obtained using a C_{60}-based molecule as the electron acceptor (1700 nA/cm^2). This result demonstrates the feasibility of using anthraquinoneanthrylacetylene-thiol linked molecule as an efficient electron acceptor for constructing a molecular monochromatic light-to-current converter.

4. ARRAYS OF WELL-DEFINED METAL-ORGANIC-METAL HETEROJUNCTIONS FOR MOLECULAR ELECTRONICS

Organic conjugated molecules are ideally suited as components in molecular electronic devices.[42] Their dimension and relative ease of preparation enable drastic miniaturization and mass production.[43] More importantly, their structures can be manipulated at the molecular level (i.e., constituents, bonding, stereochemistry) to obtain tailored electrical properties.[44–49] To obtain reproducible measurements of electron transport, organic conjugated molecules need to be covalently bonded to the electrodes—usually Au—through terminal groups such as thiols.[50–56] The imbedding of thiolated molecular assemblies in an insulating matrix of alkanethiols with gold nanoparticles (AuNPs) as top-contacts provides an attractive platform (or test-bed) for studying molecular electronics since individual AuNPs can be easily located and reliably connected with a STM tip or a conducting AFM tip.[55e, 56] Molecular assemblies from dithiols of aryl oligomers with *symmetric* structures have well-defined conformations under given self-assembly conditions.[57] In contrast, dithiols with multiple constituents and bulky moieties have *asymmetric* structures, leading to a range of intermolecular

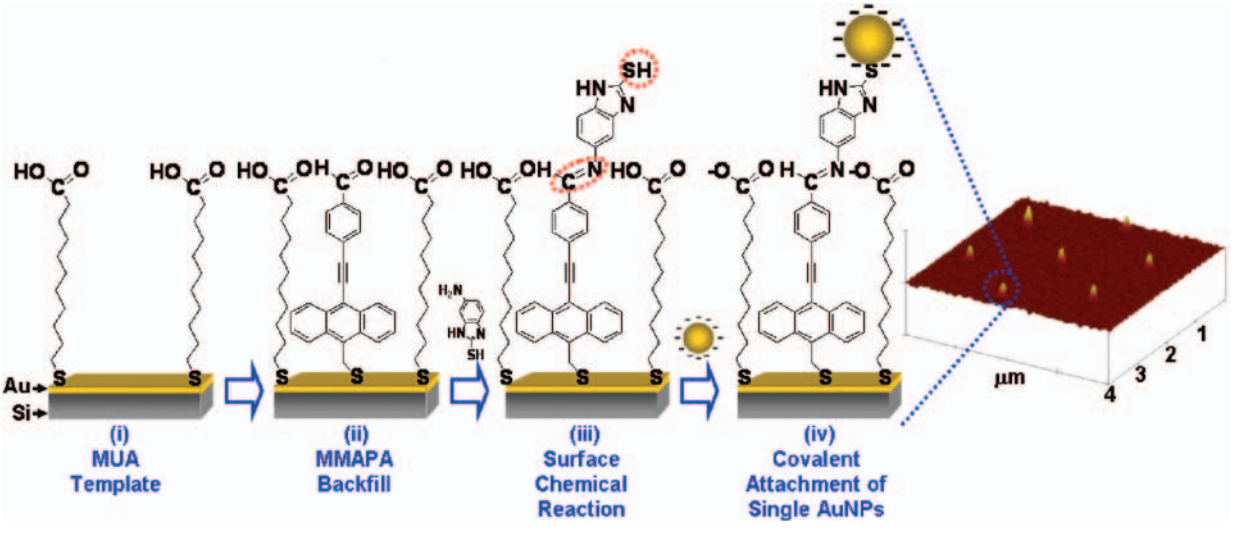

Fig. 12. Formation of thiolated molecular assemblies for the covalent attachment of single AuNPs. (i) Edge-spreading lithography of MUA molecules produced a nanopatterned gold substrate that contains hexagonal arrays of nanoholes. (ii) These nanoholes are backfilled with MMAPA molecules to create a reactive template presenting aldehyde (–CHO) end-groups. (iii) This reactive template allowed surface chemical reaction with MBIZ molecules through Schiff base (–C═N–) formation to form thiolated molecular assemblies. (iv) Under the conditions at which MUA molecules are deprotonated, assembly of negatively charged AuNPs onto thiolated molecular assemblies allowed the covalent attachment of single AuNPs as a result of the interplay of electrostatic interactions, covalent bonding, and positional constraint on the template. Reprinted with permission from [58], M. T. Zin et al., *Langmuir* 22, 6346 (**2006**). © 2006, ACS, Washington, D.C.

configurations and a considerable extent of uncertainty in conformations of molecules with respect to the electrode. However, the development of approaches to construct asymmetric molecular assemblies of relevance to molecular electronics has been limited. Furthermore, experimental procedures, providing a rapid means to fabricate addressable arrays, are necessary to conduct electrical measurements and to understand interactions between molecular assemblies.

Toward this direction, we have developed a bottom-up approach to form 2-D arrays of asymmetric molecular assemblies with covalently bonded AuNPs as potential top-contacts for electrical addressing by a scanning probe (Fig. 12).[58] We were able to achieve sub-100 nm domains of conjugated molecules insulated by alkanethiols without the need for state-of-the-art lithography. We establish a control over the structure of molecular assemblies through a combination of self-assembly processes in a layer-by-layer scheme and surface chemical reaction. As a proof-of-concept demonstration, asymmetric molecular assemblies were formed by two layers of rigid aromatic molecules with different structures. Schiff base chemistry was employed in the surface chemical reaction to selectively modify nanoscale surface features with high yield. We were able to reliably connect only one AuNP to each domain of asymmetric molecular assemblies to produce metal-organic-metal junctions of well-controlled size and interspacing.

5. INTEGRATION OF FUNCTIONAL ORGANIC MOLECULES WITH GENETICALLY ENGINEERED POLYPEPTIDES FOR NANOPARTICLE OR BIOMOLECULAR ASSEMBLY

To immobilize biomolecules onto the surfaces of synthetic materials is very important in various biotechnological applications ranging from biomedical to biochemical areas. Especially, the ability to obtain reliable and miniaturized immobilization of biomolecules is critical for biosensors, particularly for diagnostic applications. Usually, alkanethiols give homogeneous, ordered, and chemically and mechanically stable SAMs, and hence provide excellent model systems for biomaterial interfaces. However, the shortcoming of SAMs made of flexible alkyl derivative is their thermal disorder, resulting in

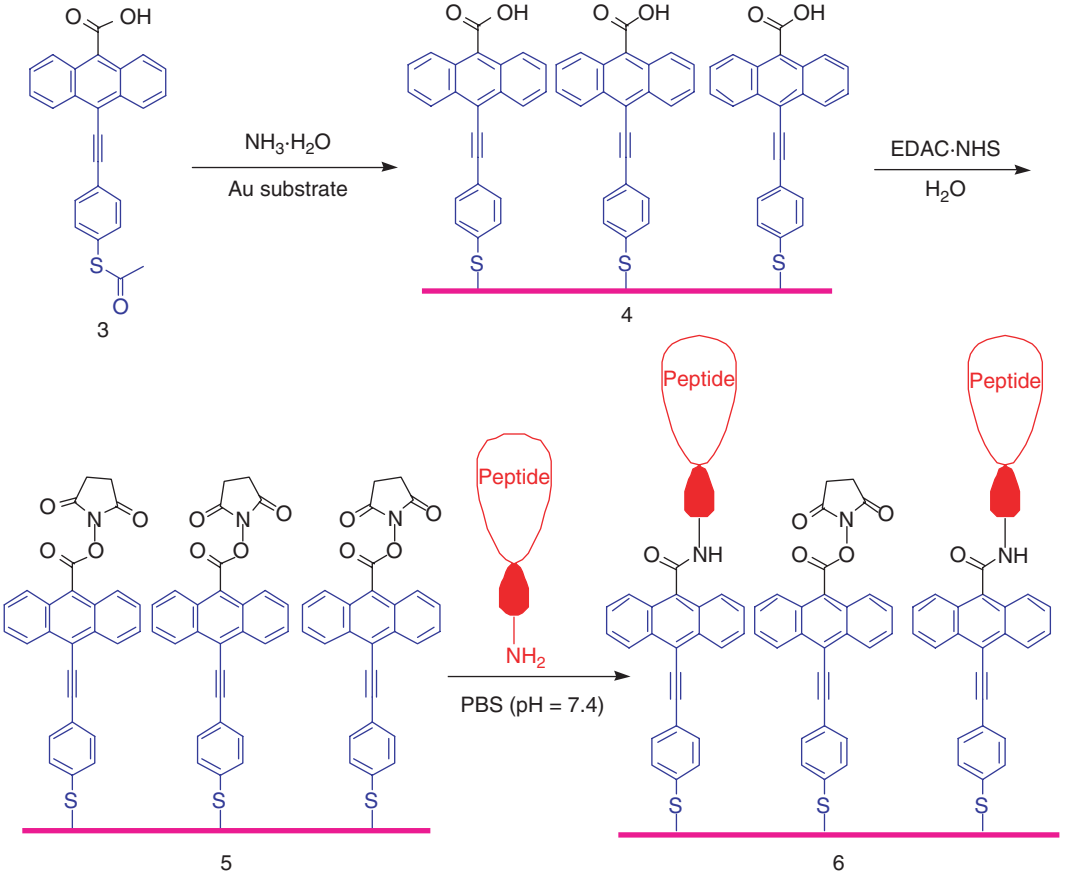

Fig. 13. Chemical immobilization of peptide onto anthryl-based self-assemblies. EDAC: 1-ethyl-3-(3-(dimethylamino)propyl)carbodiimide; NHS: *N*-hydroxysuccinimide; PBS: phosphate buffer solution; Peptide: fragments 7 to 10 of 10 units of LH-RH peptide (PGlu-His-Trp-Ser-Tyr-Gly-Leu-Arg-Pro-Gly-NH_2).

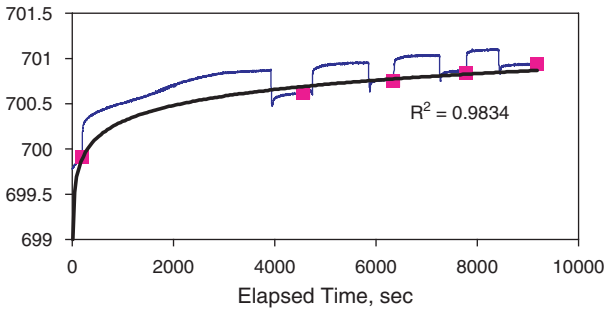

Fig. 14. SPR profile for the immobilization of peptide onto anthryl-based SAM-modified gold substrate (5 → 6). Top blue line: the adsorption process of peptide; bottom blue line: after rinsing physically adsorbed peptide; black bold line: exponential fit with the level of chemical immobilization.

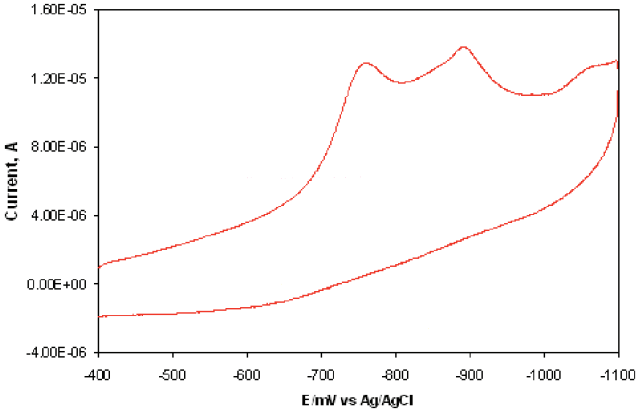

Fig. 15. Cyclic voltammetry curve for the desorption process of 6 (0.5 M KOH as the electrolyte).

surface-gauche defects and thus surface disorder. Studies of sum-frequency vibration spectroscopy show that the structure of a surface is clearly perturbed when it interacts strongly with another condensed phase, alerting us that structural perturbations need to be considered.

In our study, peptides have been chemically immobilized onto stable and highly ordered SAM template of fused-ring aromatic thiol. This was accomplished by self-assembling of the molecule 3 with ω-carboxylic end-group onto a gold substrate, activation of carboxylic acid by EDAC and NHS, and surface attachment of peptides in phosphate-buffered saline (PBS) (Fig. 13). SPR spectrum for the immobilization of peptide onto anthryl-based SAM-modified gold substrate exhibits typical exponential fit with the level of chemical immobilization (Fig. 14). The linear sweep voltammetric curve for the peptide-immobilized SAM 6 on gold substrate is shown in Figure 15. The two peaks on the reductive scan represent the desorptions of two kinds of assembled species on gold electrode. The desorption peak potential for peptide-attached SAM is more negative because of higher difficulty in the penetration of ions through the film during reduction.

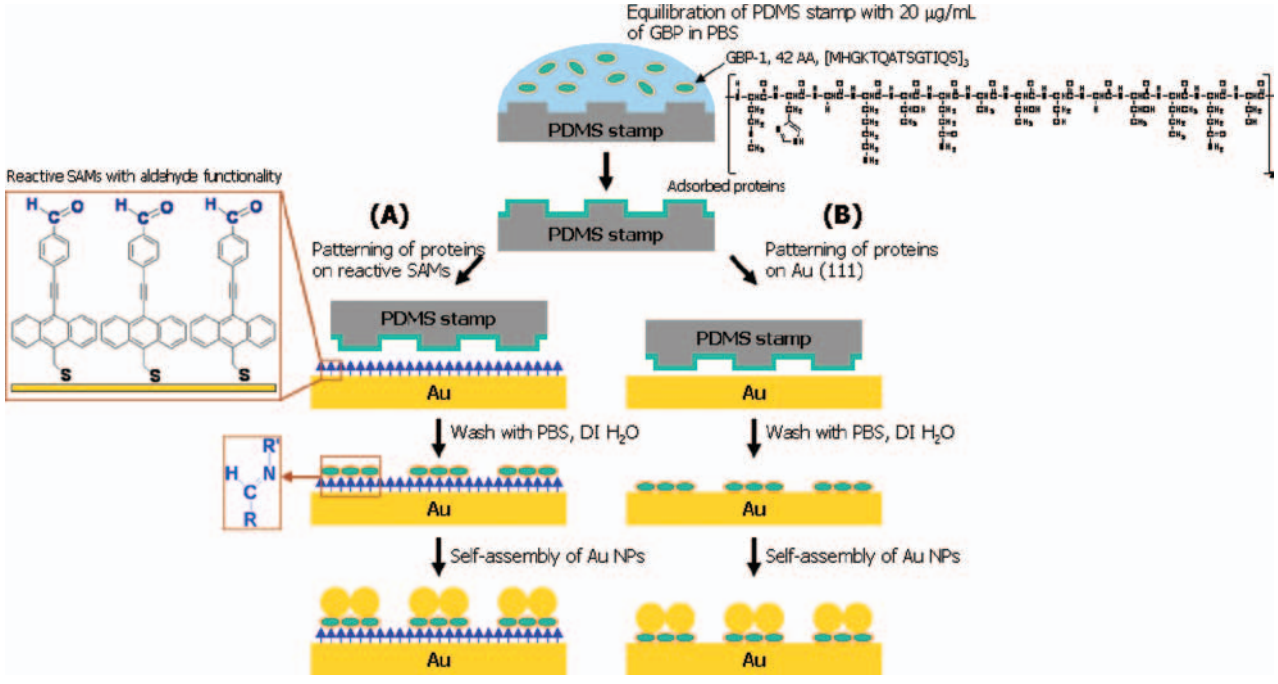

Fig. 16. Schematic representation of the experimental procedure. GBP-1 was patterned by μ-CP using two schemes. (A) GBP-1 was chemically patterned by covalent bonding between $-NH_2$ groups on the GBP-1 and –CHO end-groups of the SAMs of MMAPA through Schiff base formation. (B) GBP-1 was physically patterned onto Au(111) surface through deposition. In both cases, patterned GBP-1 function as templates to direct the assembly of gold nanoparticles. Reprinted with permission from [67], M. T. Zin et al., *Small* 1, 698 **(2005)**. © 2005, WILEY-VCH Verlag GmbH & Co., KGaA, Weinheim.

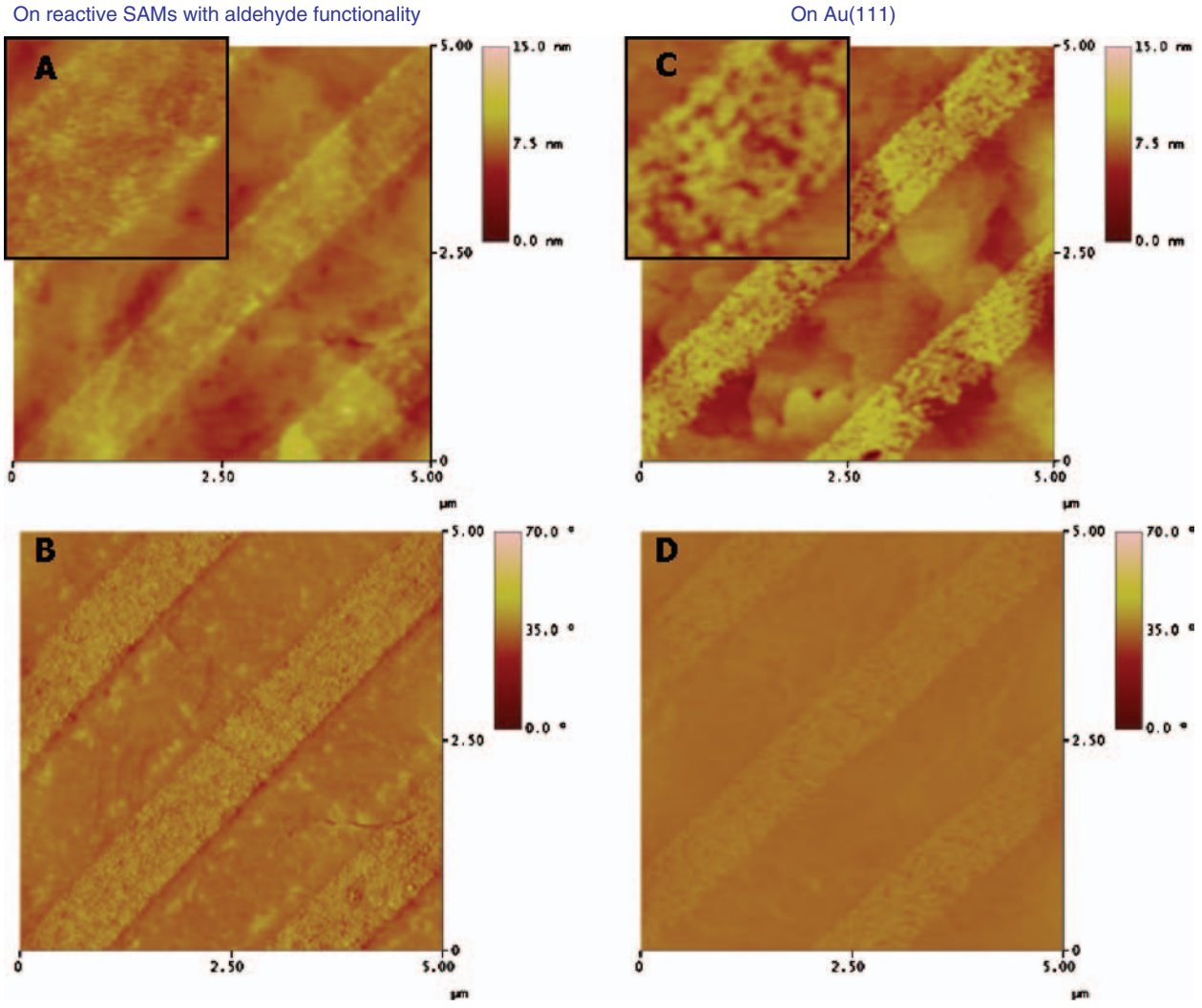

Fig. 17. Influence of surface properties on the spatial conformation of patterned GBP-1. Height (A and C) and phase (B and D) images were acquired simultaneously with AFM in tapping mode. (A–B) As a result of covalent bonding with the supporting SAMs, chemically patterned GBP-1 showed a compact morphology. GBP-1/MMAPA hybrid structures are uniform, well-packed, and highly ordered. (C–D) Physically patterned GBP-1 showed a porous morphology. Deposited GBP-1 structures are not ordered as a result of forced immobilization. Reprinted with permission from [67], M. T. Zin et al., *Small* 1, 698 **(2005)**. © 2005, WILEY-VCH Verlag GmbH & Co., KGaA, Weinheim.

In the last decade, use of phage and cell-surface display technologies has emerged as a powerful strategy to screen peptides/polypeptides with recognition for inorganic materials.[59–64] In principle, combinatorially selected polypeptides can be instrumental in not only the synthesis but also the spatial distribution of inorganic nanomaterials into functional assemblies with useful electrical and optical properties.[65] SAMs with appropriate end-groups have been patterned to produce templates for the assembly of nanoparticles through covalent bonding[66a] or electrostatic interactions.[66b] Significant advantage of combinatorially selected peptides over SAMs is their ability to identify a specific atomic composition, crystallographic orientation, or morphology of an inorganic entity. Moreover, as molecular linkers, recombinant peptides can be covalently bonded with organic functional molecules to construct hybrid superstructures which are potentially tunable in terms of physico-chemical and optoelectronic properties.[65] However, there have been no systematic studies on the fabrication of well-defined protein/organic hybrid structures on the surface or the direct patterning of genetically engineered polypeptides to assemble nanoparticles in a site-selective way. As a proof-of-concept demonstration using gold-binding polypeptide, we studied the patterning of 3-repeat engineered form of cell surface display selected gold binding peptide (GBP-1: $[MHGKTQATSGTIQS]_3$). We explored the patterning—physical or chemical—of genetically engineered polypeptides using high-resolution microcontact printing (Fig. 16).[67] In physical patterning, GBP-1 was directly transferred via deposition onto a gold substrate. In chemical patterning, GBP-1 was covalently bonded onto the pre-formed SAM with reactive end-groups. In particular, we showed that by combining microcontact printing with spatially confined surface

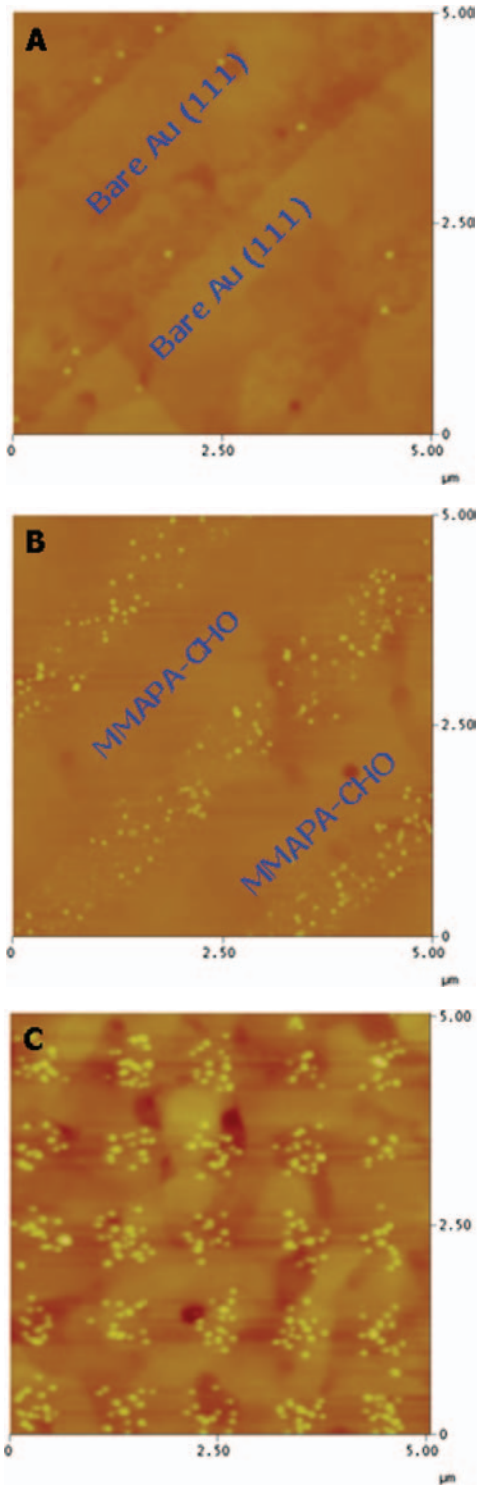

Fig. 18. Physically patterned GBP-1 (A) and chemically patterned GBP-1 (B and C) as templates in directing the assembly of gold nanoparticles. (A, B) For templates of given surface area, gold nanoparticles assembled on the chemically patterned GBP-1 in much greater number. (C) Assembled gold nanoparticles on arrays of 500 nm-wide squares—the smallest template made using μ-CP on reactive SAMs. During the assembly, no significant adsorption of gold nanoparticles in unpatterned regions was observed over a large area. Reprinted with permission from [67], M. T. Zin et al., *Small* 1, 698 **(2005)**. © 2005, WILEY-VCH Verlag GmbH & Co., KGaA, Weinheim.

chemical reaction patterns of hybrid conjugates consisting polypeptides and organic molecules can be generated simultaneously. Structural conformations of patterned GBP-1 were investigated by atomic force microscope (Fig. 17). Using patterned GBP-1 as biomimetic templates, AuNPs were directed to self-assemble into regular arrays with sub-micron dimensions (Fig. 18).

Recently, we demonstrated the utility of GBP-1 as biomolecular linkers to direct the self-assembly of CdSe@ZnS core–shell quantum dots (QDs) into 2-D arrays (Fig. 19).[68] More importantly, as the first step toward investigating plasmon-coupled photoluminescence properties of surface-immobilized peptide-QD hybrid nanoassemblies for optoelectronic and sensing applications, we showed a possibility of using peptides to tune the distance of QDs from the metal surface. Conventional approaches to assemble QDs have been based on thiol or silane linkage, hydrogen bonding, Coulombic attraction, and van der Waals forces. These interactions, however, are non-specific toward a given substrate; for example, thiols will bind indiscriminately to any metal

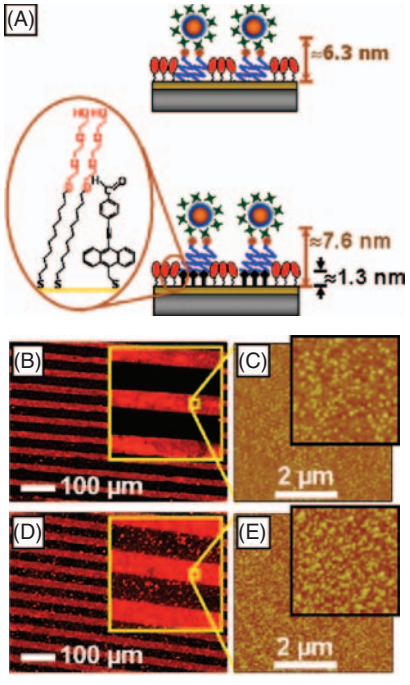

Fig. 19. (A) Schematic illustration of the attachment of QDs using biotinylated GBP-1 (top) and biotinylated GBP-1 covalently bonded to functional organic molecules (bottom) as two linkers with well-defined heights to direct the self-assembly of streptavidin functionalized CdSe@ZnS core–shell QDs. To achieve spatial control over the peptide-mediated formation of hybrid nanostructures, gold substrates patterned by μCP were used as templates. Two schemes were formulated to vary the spacing between the QDs and the gold surface (i.e., linker length) and to examine the functionality of bio-GBP-1 when covalently bonded with π-conjugated functional molecules. (B, D) From the analysis of fluorescence images, emission intensity from arrays of organic-peptide QD hybrid nanostructures was stronger. (C, E) Based on AFM results, number of QDs attached onto organic-peptide linkers was ~25% higher per unit area.

surfaces such as gold, silver, or platinum. In view of the potential of combinatorial biology technologies to identify polypeptide sequences with surface recognition for specific metals, metal oxides, or semiconductor materials, the utility of genetically engineered polypeptides for inorganics (GEPIs) as biomolecular linkers may allow new routes to the assembly of nanomaterials and formation of hybrid nanostructures on various substrates with selectivity for physical or chemical properties of the inorganic surface.

6. CONCLUSIONS AND PROSPECTS

Stable, highly ordered, and rigid SAM templates have been achieved through the development of fused-ring molecules, such as anthracene- and pyrene-based aromatic self-assembling molecules with tunable energetic (π–π stacking, hydrogen bonding, dipole–dipole interaction) and variable geometries. Based on aromatic SAM templates, highly ordered self-assembled structures of electroactive C_{60} have been obtained and shown to exhibit desirable nonlinear transporting effect for molecular electronics and efficient photocurrent generation for mimicking photosynthesis in nature. In addition, through genetically engineered polypeptides with surface recognition for specific inorganics, the patterned assembly of nanoparticles onto aromatic SAM templates has been realized through a combination of μ-CP and spatially confined surface chemical reaction.

Besides fullerenes and carbon nanotubes, metal (e.g., Au and Ag), semiconductor (e.g., CdS, CdSe, ZnS, PbS, GaAs, and Si) and metal oxide (e.g., Fe_2O_3, SiO_2, and TiO_2) nanoparticles and nanowires are certain to play an important role as fundamental building blocks to construct next generation of nanoscale electronic, optical, and sensing devices. However, there are numerous challenges and questions which must be addressed before novel applications based on unique properties of nanomaterials can be successfully implemented. Besides efficient preparation and stabilization of nanomaterials, new methods for assembling nanomaterials into stable and highly ordered arrays with complex electronic, photonic, or sensing functions are required. Combination of aromatic SAM templates with adjustable nanoscale features and biomolecules such as proteins and DNAs will be a versatile strategy to assemble nanomaterials.

Acknowledgments: This work was supported by ARO-DURINT, the Air Force Office of Scientific Research (AFOSR) under the Bioinspired Concept Program, and Genetically Engineered Materials Science and Engineering Center, the NSF-MRSEC at the University of Washington. Alex K.-Y. Jen thanks the Boeing-Johnson Foundation for its support. Melvin T. Zin thanks the Center for Nanotechnology at the University of Washington for its UIF Graduate Fellowship.

References and Notes

1. (a) A. P. Alivisatos, *Science* 271, 933 (**1996**); (b) W. J. Parak, D. Gerion, T. Pellegrino, D. Zanchet, C. Micheel, S. C. Williams, R. Boudreau, M. A. L. Gros, C. A. Larabell, and A. P. Alivisatos, *Nanotechnology* 14, R15 (**2003**); (c) M. A. El-sayed, *Acc. Chem. Res.* 37, 326 (**2004**); (d) M.-C. Daniel and D. Astruc, *Chem. Rev.* 104, 293 (**2004**); (e) C. Burda, X. B. Chen, R. Narayanan, and M. A. El-Sayed, *Chem. Rev.* 105, 1025 (**2005**); (f) Y. N. Xia, P. D. Yang, Y. G. Sun, Y. Y. Wu, B. Mayers, B. Gates, Y. D. Yin, F. Kim, and H. Q. Yan, *Adv. Mater.* 15, 353 (**2003**).
2. (a) C. A. Mirkin and W. B. Caldwell, *Tetrahedron* 52, 5113 (**1996**); (b) M. Prato, *Chem. Soc. Rev.* 28, 263 (**1999**).
3. (a) D. Tass, N. Tagmatarchis, V. Georgakilas, and M. Prato, *Chem. Eur. J.* 9, 4001 (**2003**); (b) P. Avouris, *Acc. Chem. Res.* 35, 1026 (**2002**); (c) R. H. Baughman, A. A. Zakhidov, and W. A. de Heer, *Science* 297, 787 (**2002**).
4. (a) F. Vögtle, S. Gestermann, R. Hesse, H. Schwierz, and B. Windisch, *Prog. Polym. Sci.* 25, 987 (**2000**); (b) D. A. Tomalia and J. M. J. Frechet, *J. Polym. Sci., Polym. Chem.* 40, 2719 (**2002**); (c) A. D. Schlüter and J. P. Rabe, *Angew. Chem. Int. Ed.* 39, 864 (**2000**).
5. (a) G. M. Whitesides and B. Crzybowski, *Science* 295, 2418 (**2002**); (b) F. Schreiber, *Prog. Surf. Sci.* 65, 151 (**2000**); (c) R. K. Smith, P. A. Lewis, and P. S. Weiss, *Prog. Surf. Sci.* 75, 1 (**2004**); (d) E. Katz and I. Willner, *Angew. Chem. Int. Ed.* 43, 6042 (**2004**); (e) C. M. Niemeyer, *Angew. Chem. Int. Ed.* 40, 4128 (**2001**); (f) H. Colfen and S. Mann, *Angew. Chem. Int. Ed.* 42, 2350 (**2003**); (g) J. C. Love, L. A. Estroff, J. K. Kriebel, R. G. Nuzzo, and G. M. Whitesides, *Chem. Rev.* 105, 1103 (**2005**).
6. A. Ulman, *Chem. Rev.* 96, 1533 (**1996**).
7. R. W. Carpick and M. Salmeron, *Chem. Rev.* 97, 1163 (**1997**).
8. E. Ostuni, L. Yan, and G. M. Whitesides, *Colloid Surf. B: Biointerf.* 15, 3 (**1999**).
9. K. E. Nelson, L. Gamble, L. S. Jung, M. S. Boeckl, E. Naeemi, S. L. Golledge, T. Sasaki, D. G. Castner, C. T. Campbell, and P. S. Stayton, *Langmuir* 17, 2807 (**2001**).
10. M. Mrksich, *Chem. Soc. Rev.* 29, 267 (**2000**).
11. A. Ulman, *Acc. Chem. Res.* 34, 855 (**2001**).
12. (a) A. R. Bishop and R. G. Nuzzo, *Curr. Opin. Coll. Interf. Sci.* 1, 127 (**1996**); (b) S. Okada, S. Peng, W. Spevak, and D. Charych, *Acc. Chem. Res.* 31, 229 (**1998**); (c) V. Chechik, R. M. Crooks, and J. M. Stirling, *Adv. Mater.* 12, 1161 (**2000**).
13. (a) A. Salomon, D. Cahen, S. Lindsay, J. Tomfohr, V. B. Engelkes, and C. D. Frisbie, *Adv. Mater.* 15, 1881 (**2003**); (b) R. A. Wassel and C. B. Gorman, *Angew. Chem. Int. Ed.* 43, 5120 (**2004**).
14. (a) L. A. Bumm, J. J. Arnold, M. T. Cygan, T. D. Dunbar, T. P. Burgin, L. Jones II, D. L. Allara, J. M. Tour, and P. S. Weiss, *Science* 271, 1705 (**1996**); (b) J. G. Kushmerick, D. B. Holt, S. K. Pollack, M. A. Ratner, J. C. Yang, T. L. Schull, J. Naciri, M. H. Moore, and R. Shashidhar, *J. Am. Chem. Soc.* 124, 10654 (**2002**).
15. R. M. Metzgerm, *Acc. Chem. Res.* 32, 950 (**1999**). (b) M. A. Fox, *Acc. Chem. Res.* 32, 201 (**1999**).
16. J. Chen, M. A. Reed, A. M. Rawlett, and J. M. Tour, *Science* 286, 1550 (**1999**).
17. (a) C. O. Collier, G. Mattersteig, E. W. Wong, Y. Luo, K. Beverly, J. Sampaio, F. M. Raymo, J. F. Stoddart, and J. R. Heath, *Science* 289, 1172 (**2000**); (b) Z. J. Donhauser, B. A. Mantooth, K. F. Kelly, L. A. Bumm, J. D. Monnell, J. J. Stapleton, D. W. Price, Jr., A. M. Rawlett, D. L. Allara, J. M. Tour, and P. S. Weiss, *Science* 292, 2303 (**2001**).
18. (a) M. A. Reed, C. Zhou, C. J. Muller, T. P. Burgin, and J. M. Tour, *Science* 278, 252 (**1997**); (b) J. K. Gimzewski and C. Joachim, *Science* 283, 1683 (**1999**); (c) D. A. Krapchetov, H. Ma, A. K.-Y. Jen, D. A. Fischer, and Y. L. Loo, *Langmuir* 21, 5887 (**2005**).
19. (a) D. M. Adams, L. Brus, C. E. D. Chidsey, S. Creager, C. Creutz, C. R. Kagan, P. V. Kamat, M. Lieberman, S. Lindsay, R. A. Marcus,

R. M. Metzger, M. E. Michel-Beyerle, J. R. Miller, M. D. Newton, D. R. Rolison, O. Sankey, K. S. Schanze, J. Yardley, and X. Y. Zhu, *J. Phys. Chem. B* 107, 6668 **(2003)**; (b) H. Yamada, H. Imahori, Y. Nishimura, I. Yamazaki, and S. Fukuzumi, *Adv. Mater.* 14, 892 **(2002)**; (c) F. B. Abdelrazzaq, R. C. Kwong, and M. E. Thompson, *J. Am. Chem. Soc.* 124, 4796 **(2002)**.

20. L. S. Jung, K. E. Nelson, P. S. Stayton, and C. T. Campbell, *Langmuir* 16, 9421 **(2000)**.

21. (a) M. Prato, *J. Mater. Chem.* 7, 1097 **(1997)**; (b) G. Yu, J. Gao, J. C. Hummelen, F. Wudl, and A. J. Heeger, *Science* 270, 1789 **(1995)**.

22. (a) X. Shi, W. B. Caldwell, K. Chen, and C. A. Mirkin, *J. Am. Chem. Soc.* 116, 11598 **(1994)**; (b) O. Dominguez, L. Echegoyen, F. Cunha, and N. J. Tao, *Langmuir* 14, 821 **(1998)**; (c) L. F. Yuan, J. Yang, H. Wang, C. Zeng, Q. Li, B. Wang, J. G. Hou, Q. Zhu, and D. M. Chen, *J. Am. Chem. Soc.* 125, 169 **(2003)**.

23. M. H. Zareie, H. Ma, B. W. Reed, A. K.-Y. Jen, and M. Sarikaya, *Nano Lett.* 3, 139 **(2003)**.

24. J. L. Bredas, J. P. Calbert, D. A. Filho, and J. Cornil, *PNAS* 99, 5804 **(2002)**.

25. (a) F. Rosei, M. Schunack, P. Jiang, A. Gourdon, E. Lagsgaard, I. Stensgaard, C. Joachim, and F. Besenbacher, *Science* 296, 328 **(2002)**; (b) T. Vondrak, C. J. Cramer, and X. Y. Zhu, *J. Phys. Chem. B* 103, 8915 **(1999)**; (c) J. M. Beebe, V. B. Engelkes, L. L. Miller, and C. D. Frisbie, *J. Am. Chem. Soc.* 124, 11268 **(2002)**.

26. S. H. Kang, H. Ma, M.-S. Kang, K.-S. Kim, A. K.-Y. Jen, M. H. Zareie, and M. Sarikaya, *Angew. Chem. Int. Ed.* 43, 1512 **(2004)**.

27. H. Imahori, T. Azuma, A. Ajavakom, H. Norieda, H. Yamada, and Y. Sakaya, *J. Phys. Chem. B* 103, 7233 **(1999)**.

28. L. Echegoyen and L. E. Echegoyen, *Acc. Chem. Res.* 31, 593 **(1998)**.

29. R. J. Willson, G. Meijer, D. S. Bethune, R. D. Johnson, D. D. Chambliss, M. S. de Vries, H. E. Hunziker, and H. R. Wendt, *Nature* 348, 621 **(1990)**.

30. L. D. Lamb, D. R. Huffman, R. K. Workman, S. Howells, T. Chen, D. Sarid, and R. F. Ziolo, *Science* 255, 1413 **(1992)**.

31. E. I. Altman and R. J. Colton, *Phys. Rev. B* 48, 18244 **(1993)**.

32. W. B. Caldwell, K. Chen, C. A. Mirkin, and S. J. Babinec, *Langmuir* 9, 1945 **(1993)**.

33. V. V. Tsukruk, L. M. Lander, and W. J. Brittain, *Langmuir* 10, 996 **(1994)**.

34. F. Arias, L. A. Godínez, S. R. Wilson, A. E. Kaifer, and L. Echegoyen, *J. Am. Chem. Soc.* 118, 6086 **(1996)**.

35. Y.-S. Shon, K. F. Kelly, N. J. Halas, and T. R. Lee, *Langmuir* 15, 5329 **(1999)**.

36. S. Zhang, D. Dong, L. Gan, Z. Liu, and C. Huang, *New J. Chem.* 25, 606 **(2001)**.

37. (a) T. Sakurai, X. D. Wang, K. Q. Xue, Y. Hasegawa, T. Hashizume, and H. Shinohara, *Prog. Surf. Sci.* 51, 263 **(1996)**; (b) A. Machenko and J. Cousty, *Surf. Sci.* 513, 233 **(2002)**.

38. J. G. Hou, J. L. Yang, H. Q. Wang, Q. X. Li, C. G. Zeng, L. F. Yuan, B. Wang, D. M. Chen, and Q. S. Zhu, *Nature* 409, 304 **(2001)**.

39. (a) J. Chen, M. A. Reed, A. M. Rawlett, and J. M. Tour, *Science* 286, 1550 **(1999)**; (b) Y. Selzer, A. Salomon, J. Ghabboun, and D. Cahen, *Angew. Chem. Int. Ed.* 41, 827 **(2002)**; (c) C. B. Gorman, R. L. Carroll, and R. R. Fuierer, *Langmuir* 17, 6923 **(2001)**; (d) J. Cornil, Y. Karzazi, and J. L. Brédas, *J. Am. Chem. Soc.* 124, 3516 **(2002)**.

40. (a) M.-S. Kang, S. H. Kang, H. Ma, K.-S. Kim, and A. K.-Y. Jen, *J. Power Sources* **(2006)**, in press; (b) K.-S. Kim, M.-S. Kang, H. Ma, and A. K.-Y. Jen, *Chem. Mater.* 16, 5058 **(2004)**.

41. H. Ma, M.-S. Kang, Q. M. Xu, K.-S. Kim, and A. K.-Y. Jen, *Chem. Mater.* 17, 2896 **(2005)**.

42. (a) A. Aviram and M. A. Ratner, *Chem. Phys. Lett.* 29, 277 **(1974)**; (b) C. A. Mirkin and M. A. Ratner, *Annu. Rev. Phys. Chem.* 43, 719 **(1992)**; (c) M. A. Reed, *Proc. IEEE* 87, 652 **(1999)**; (d) C. Joachim, J. K. Gimzewski, and A. Aviram, *Nature* 408, 541 **(2000)**; (e) R. A. Wassel and C. B. Gorman, *Angew. Chem. Int. Ed.* 43, 5120 **(2004)**.

43. J. M. Tour, *Acc. Chem. Res.* 33, 791 **(2000)**.

44. (a) C. Patoux, J.-P. Launay, M. Beley, Chodorowski-Kimmes, J.-P. Collin, S. James, and J.-P. Sauvage, *J. Am. Chem. Soc.* 120, 3717 **(1998)**; (b) W. B. Davis, W. A. Svec, M. A. Ratner, and M. R. Wasielewski, *Nature* 396, 60 **(1998)**.

45. (a) N. J. Geddes, J. R. Sambles, D. J. Davis, W. G. Parker, and D. J. Sandman, *Appl. Phys. Lett.* 56, 1916 **(1990)**; (b) D. H. Waldeck and D. N. Beratan, *Science* 261, 576 **(1993)**; (c) R. M. Metzger, B. Chen, M. V. Lakshmikantham, D. Vuillaume, T. Kawai, X. Wu, H. Tachibana, T. V. Hughes, H. Sakurai, J. W. Baldwin, C. Hosch, M. P. Cava, L. Brehmer, and G. J. Ashwell, *J. Am. Chem. Soc.* 119, 10455 **(1997)**.

46. (a) A. R. Pease, J. O. Jeppesen, J. F. Stoddart, Y. Luo, C. P. Collier, and J. R. Heath, *Acc. Chem. Res.* 34, 433 **(2001)**; (b) S. Fraysse, C. Coudret, and J.-P. Launay, *Eur. J. Inorg. Chem.* 7, 1581 **(2000)**.

47. (a) A. J. Aviram, *J. Am. Chem. Soc.* 110, 5687 **(1998)**; (b) J. Chen and M. A. Reed, *Appl. Phys. Lett.* 78, 3735 **(2001)**.

48. T. Osa and M. Fujihira, *Nature* 264, 349 **(1976)**.

49. C. Joachim and J. K. Gimzeswski, *Phys. Rev. Lett.* 74, 2102 **(1995)**.

50. J. Chen, M. A. Reed, A. M. Rawlett, and J. M. Tour, *Science* 286, 1550 **(1999)**.

51. M. A. Reed, C. Zhou, C. J. Muller, T. P. Burgin, and J. M. Tour, *Science* 278, 252 **(1997)**.

52. (a) H. Park, J. Park, A. K. L. Kim, E. H. Anderson, P. A. Alivisatos, and P. L. McEuen, *Nature* 407, 57 **(2000)**; (b) Y. Selzer, M. A. Cabassi, T. S. Mayer, and D. L. Allara, *J. Am. Chem. Soc.* 126, 4052 **(2004)**.

53. J. K. N. Mbindyo, T. E. Mallouk, J. B. Mattzela, I. Kratochvilova, B. Razavi, T. N. Jackson, and T. S. Mayer, *J. Am. Chem. Soc.* 124, 4020 **(2002)**.

54. (a) R. E. Holmlin, R. Haag, M. L. Chabinyc, R. F. Ismagilov, A. E. Cohen, A. Terfort, M. A. Rampi, and G. M. Whitesides, *J. Am. Chem. Soc.* 123, 5075 **(2001)**; (b) Y. Selzer, A. Salomon, and D. Cahen, *J. Phys. Chem. B* 106, 10432 **(2002)**; (c) Y.-L. Liu and H.-Z. Yu, *Chem. Phys. Chem.* 19, 799 **(2002)**.

55. (a) R. P. Andres, T. Bein, M. Dorogi, S. Feng, J. I. Henderson, C. P. Kubiak, W. Mahoney, R. G. Osifchin, and R. Reifenberger, *Science* 272, 1323 **(1996)**; (b) D. I. Gittins, D. Bethell, D. J. Schiffrin, and R. J. Nichols, *Nature* 408, 67 **(2000)**; (c) F.-R. F. Fan, J. Yang, S. M. Dirk, D. W. Price, D. Kosynkin, J. M. Tour, and A. J. Bard, *J. Am. Chem. Soc.* 123, 2454 **(2001)**; (d) B. Xu and N. J. Tao, *Science* 301, 1221 **(2003)**; (e) A. S. Blum, J. G. Kushmerick, D. P. Long, C. H. Patterson, J. C. Yang, J. C. Henderson, Y. Yao, J. M. Tour, R. Shashidhar, and B. R. Ratna, *Nat. Mater.* 4, 167 **(2005)**.

56. X. D. Cui, A. Primak, X. Zarate, J. Tomfohr, O. F. Sankey, A. L. Moore, T. A. Moore, D. Gust, G. Harris, and S. M. Lindsay, *Science* 294, 571 **(2001)**.

57. (a) J. Stapleton, P. Harder, T. Daniel, M. D. Reinard, Y. Yao, D. Price, J. M. Tour, and D. L. Allara, *Langmuir* 19, 8245 **(2003)**; (b) L. J. Richter, C. S.-C. Yang, P. T. Wilson, C. A. Hacker, R. D. van Zee, J. J. Stapleton, D. L. Allara, and J. M. Tour, *J. Phys. Chem. B* 108, 12547 **(2004)**.

58. M. T. Zin, H. Yip, N. Wong, H. Ma, and A. K.-Y. Jen, *Langmuir* 22, 6346 **(2006)**.

59. (a) S. Brown, *Proc. Natl. Acad. Sci. USA* 89, 8651 **(1992)**; (b) S. Brown, *Nat. Biotechnol.* 15, 269 **(1997)**; (c) S. Brown, M. Sarikaya, and E. Johnson, *J. Mol. Biol.* 299, 725 **(2000)**.

60. S. R. Whaley, D. S. English, E. L. Hu, P. F. Barbara, and A. M. Belcher, *Nature* 405, 665 **(2000)**.

61. R. R. Naik, L. Brott, S. J. Carlson, and M. O. Stone, *J. Nanosci. Nanotechnol.* 2, 95 **(2002)**.

62. S. Nygaard, R. Wendelbo, and S. Brown, *Adv. Mater.* 14, 1853 **(2002)**.

63. K. Goede, P. Busch, and M. Grundmann, *Nano Lett.* 4, 2115 **(2004)**.

64. (a) C. K. Thai, H. X. Dai, M. S. R. Sastry, M. Sarikaya, D. T. Schwartz, and F. Baneyx, *Biotechnol. Bioeng.* 8, 129 **(2004)**; (b) H. Dai, C. K. Thai, M. Sarikaya, F. Baneyx, and D. T. Schwartz, *Langmuir* 20, 3483 **(2004)**.

65. (a) M. Sarikaya, C. Tamerler, A. K.-Y. Jen, K. Schulten, and F. Baneyx, *Nat. Mater.* 2, 577 **(2003)**; (b) M. Sarikaya, C. Tamerler, D. T. Schwartz, and F. Baneyx, *Annu. Rev. Mater. Res.* 34, 373 **(2004)**.

66. (a) L. Yan, X.-M. Zhao, and G. M. Whitesides, *J. Am. Chem. Soc.* 120, 6179 **(1998)**; (b) P. M. Mendes, S. Jacke, K. Critchley, J. Plaza, Y. Chen, K. Nikitin, R. E. Palmer, J. A. Preece, S. D. Evans, and D. Fitzmaurice, *Langmuir* 20, 3766 **(2004)**. For studies on the interaction between SAMs and nanoparticles, please refer to the following papers: V. L. Colvin, A. N. Goldsterin, and A. P. Alivisatos, *J. Am. Chem. Soc.* 114, 5221 **(1992)**; S. Ogawa, F. F. Fan, and A. J. Bard, *J. Phys. Chem.* 99, 1182 **(1995)**; R. Rizza, D. Fitzmaurice, S. Hearne, G. Hughes, G. Spoto, E. Ciliberto, H. Kerp, and R. Schropp, *Chem. Mater.* 9, 2969 **(1997)**.

67. M. T. Zin, H. Ma, M. Sarikaya, and A. K.-Y. Jen, *Small* 1, 698 **(2005)**.

68. M. T. Zin, A. M. Munro, M. Gungormus, H. Ma, C. Tamerler, D. S. Ginger, M. Sarikaya, and A. K.-Y. Jen, *J. Mater. Chem.* 17, 866 **(2007)**.

Received: 26 August 2006. Accepted: 13 November 2006.